Time-Domain Generalized Transition Matrix for Transient Scattering Analysis of Arrays

Xuezhe Tian, *Student Member, IEEE*, Gaobiao Xiao, *Member, IEEE*, and Shang Xiang, *Student Member, IEEE*

***Abstract*—Time-domain generalized transition matrix (TD-GTM) based on the time-domain integral equations (TDIEs) is implemented in this letter. The TD-GTM is established on the reference Huygens surface that encloses the object, using the impulse responses obtained by the marching-on-in-time (MOT) solutions. The TD-GTM fulfills the domain decomposition of TDIEs naturally and flexibly. It allows us to analyze each module independently and then to solve the whole system by establishing the time-domain generalized surface integral equation (TD-GSIE). Various TDIEs are used to extract the TD-GTM for different modules. Numerical results show that the TD-GTM can effectively improve the efficiency of original TDIEs for transient scattering analysis of array structures.**

***Index Terms*—Arrays, domain decomposition method, marching on in time (MOT), time-domain generalized surface integral equation (TD-GSIE), time-domain generalized transition matrix (TD-GTM), time-domain integral equations (TDIEs).**

I. Introduction

GIVEN the variety of electromagnetic compatibility/interference (EMC/EMI) effects involved in modern electronic systems, numerical analysis of such systems using a single integration scheme is clearly prohibitive. The domain decomposition method (DDM) is a feasible solution that allows us to divide the whole complex and large-scale system into subdomains, and electromagnetic fields of each subdomain can be solved independently. For the method of moments (MoM), generalized transition matrix algorithm (GTM) [1], [2], equivalence principle algorithm (EPA) [3], nonconformal DDM [4], and the linear embedding via Green's operators (LEGO) [5]–[7] have manifested their superiority in analyzing complex systems, such as phased antenna arrays, band-gap structures, coupled components in integrated packages, as well as anisotropic bodies. Meanwhile, DDM in the time domain for time-domain integral equations (TDIEs) remains largely to be investigated and developed.

In this letter, we are aiming to implement DDM for the TDIEs, using the time-domain generalized transition matrix algorithm (TD-GTM) and time-domain generalized surface integral equation (TD-GSIE). We define the TD-GTM on a reference surface uniquely to characterize the time-domain electromagnetic properties of each module. It directly relates the rotated tangential components of the scattered fields to the rotated tangential components of the incident fields. This relationship can be obtained using the impulse responses of the TDIEs inside the equivalent surface, when the inside solver is free from the resonance problems [8]. Wideband time domain information can be incorporated in the TD-GTM, which is a great superiority to the frequency GTM. After extraction, the TD-GTM is used to establish TD-GSIE for the whole system, where coupling effects among all subdomains are considered.

Manuscript received April 14, 2015; accepted May 24, 2015. Date of publication June 01, 2015; date of current version February 12, 2016. This work was supported by the National Science Foundation of China under Grant 61234001 and the SAST Foundation 2013.

The authors are with Shanghai Jiao Tong University, Shanghai 200240, China (e-mail: smarter@sjtu.edu.cn).

Color versions of one or more of the figures in this letter are available online at http://ieeexplore.ieee.org.

Digital Object Identifier 10.1109/LAWP.2015.2439057

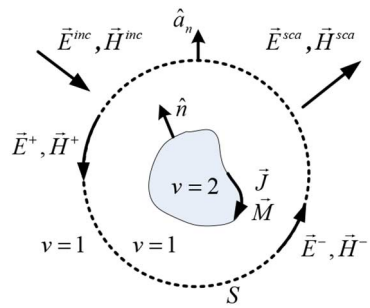

Fig. 1. A scatterer enclosed by the Huygens surface.

II. Theory of the Time-Domain Generalized Transition Matrix

In general, the TD-GTM is an extension of the GTM in the frequency domain. Consider a scatterer enclosed by the Huygens surface S, as is shown in Fig. 1. The incident fields are denoted as $\vec{E}^{\rm inc}$, $\vec{H}^{\rm inc}$. Their rotated tangential components on the equivalent surface are $\vec{E}^{+}$, $\vec{H}^{+}$ respectively, which read

$$\begin{bmatrix} \vec{E}^{+} \\ \eta\vec{H}^{+} \end{bmatrix} = \begin{bmatrix} \vec{E}^{\rm inc} \times \hat{a}_n \\ \hat{a}_n \times \eta\vec{H}^{\rm inc} \end{bmatrix}. \tag{1}$$

Here, $\hat{a}_n$ is the outward unit normal of the equivalent surface, and η is the intrinsic impedance of the free space.

To represent the fields $\vec{E}^{\rm rad}$ and $\vec{H}^{\rm rad}$ radiated in the region-ν by the surface equivalent electric currents $\vec{J}_{\rm s}$ and magnetic currents $\vec{M}_{\rm s}$, we define an operator matrix $[\mathcal{S}_\nu]$ as

$$\begin{bmatrix} \vec{E}^{\rm rad} \times \hat{n} \\ \hat{n} \times \eta\vec{H}^{\rm rad} \end{bmatrix} = [\mathcal{S}_\nu] \begin{bmatrix} \vec{M}_{\rm s} \\ \eta\vec{J}_{\rm s} \end{bmatrix} \tag{2}$$

in which

$$[\mathcal{S}_\nu] = \begin{bmatrix} \mathcal{K}_\nu^M & -\eta^{-1}\mu_\nu\mathcal{L}_\nu^J \\ \eta\varepsilon_\nu\mathcal{L}_\nu^M & \mathcal{K}_\nu^J \end{bmatrix}. \tag{3}$$

$\mathcal{L}_\nu$ and $\mathcal{K}_\nu$ are the electric field integral operator and the magnetic field integral operator, respectively, as defined in [9]. μ_ν

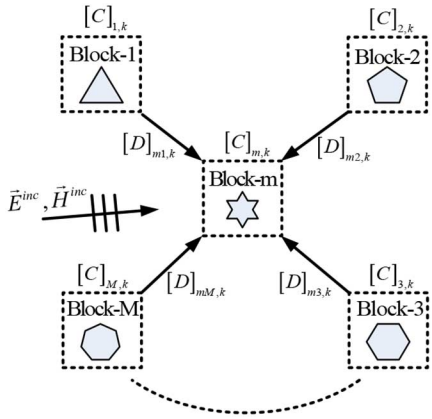

Fig. 2. Total field imposed on the mth block in a multimodule system.

is the permeability, and ε_ν represents permittivity in region-ν ($\nu = 1$ denotes the free space).

The rotated tangential fields imposed on the objects inside the closed surface can be regenerated by $\vec{E}^+$ and $\vec{H}^+$ as follows:

$$\begin{bmatrix} \vec{E}^i \times \hat{n} \\ \hat{n} \times \eta\vec{H}^i \end{bmatrix} = -[\mathcal{S}_1] \begin{bmatrix} \vec{E}^+ \\ \eta\vec{H}^+ \end{bmatrix}. \tag{4}$$

Then, equivalent electric and magnetic currents $\vec{J}$ and $\vec{M}$ on the enclosed objects can be solved using the marching-on-in-time (MOT) procedure based on specific TDIEs. They will generate the outgoing fields, whose rotated tangential components on S can be denoted by

$$\begin{bmatrix} \vec{E}^- \\ \eta\vec{H}^- \end{bmatrix} = [\mathcal{S}_1] \begin{bmatrix} \vec{M} \\ \eta\vec{J} \end{bmatrix}. \tag{5}$$

The fields $\vec{E}^{\rm sca}$ and $\vec{H}^{\rm sca}$ outside S can be easily obtained from $\vec{E}^-$ and $\vec{H}^-$. To get the TD-GTM of the module is to find out the relation between the ingoing and outgoing rotated tangential field variables $\vec{E}^+$, $\vec{H}^+$ and $\vec{E}^-$, $\vec{H}^-$. The establishment of inner TDIE solvers is not elaborated here. Interested readers can find more details in [9]–[11]. After the discretization and testing procedure, we can express the relationship between the discretized outgoing variables $e^-_{n,j}h^-_{n,j}$ and the discretized incident variables $e^{\rm inc}_{n,j}h^{\rm inc}_{n,j}$ in a convolution way

$$\begin{bmatrix} e^- \\ \eta h^- \end{bmatrix}_j = \sum_{k=0}^{k^c_{\max}-1} [C]_k \begin{bmatrix} e^{\rm inc} \\ \eta h^{\rm inc} \end{bmatrix}_{j-k} + Q^c_{j-k^c_{\max}} \tag{6}$$

in which

$$Q^c_{j-k^c_{\max}} = Q^c_{j-k^c_{\max}-1} + [C]_{k^c_{\max}} \begin{bmatrix} e^{\rm inc} \\ \eta h^{\rm inc} \end{bmatrix}_{j-k^c_{\max}}.$$

Here, $[C]_k$ ($k = 0, 1, \cdots, k^c_{\max}$) are defined as the time-domain generalized transition matrices, denoted as TD-GTM. $k^c_{\max}$ is the length of $[C]_k$. To obtain the TD-GTM, we set $e^{\rm inc}_k$ and $h^{\rm inc}_k$ to be the delta-like impulses [8]

$$\begin{bmatrix} e^{\rm inc} \\ \eta h^{\rm inc} \end{bmatrix}_k = \begin{cases} \delta_m & k = 0 \\ 0 & \text{else} \end{cases}, \quad m = 1, 2, \cdots, N_{\rm es} \tag{7}$$

in which $N_{\rm es}$ is the number of unknowns on the equivalent surface, δ_m is a column vector, and its entries are

$$\delta_m(n) = \begin{cases} 1 & n = m \\ 0 & \text{else} \end{cases}, \quad n = 1, 2, \cdots, N_{\rm es}.$$

It should be emphasized that the inner solver for the TD-GTM extraction should be resonance-free. $k^c_{\max}$ will be very large if the impulse responses contain highly resonance components. To determine a reasonable $k^c_{\max}$, we define the sample length ratio ($r_{\rm sl}$), which equals the ratio between $k^c_{\max}\Delta t$ and the time that wave travels in the longest path inside S.

III. Implementation of the TD-GSIE

For a multimodule system, TD-GSIE can be established based on TD-GTM of each block and the coupling among them.

Consider a multiradiating structure as shown in Fig. 2. We separate it into M elements and enclose each element by a regular equivalent surface. The interactions between the original elements are conveyed through their reference surfaces. The total fields imposed on the mth module consist of two parts, the incident fields and the coupling fields from other modules

$$\begin{bmatrix} \vec{E}^+ \\ \eta\vec{H}^+ \end{bmatrix}_m = \begin{bmatrix} \vec{E}^{\rm inc} \times \hat{a}_n \\ \hat{a}_n \times \eta\vec{H}^{\rm inc} \end{bmatrix}_m + \sum_{n=1, n\neq m}^{M} [\mathcal{S}_1]_{m,n} \begin{bmatrix} \vec{E}^- \\ \eta\vec{H}^- \end{bmatrix}_n \tag{8}$$

in which $[\mathcal{S}_1]_{m,n}$ is the operator matrix in (3) that transmits the interaction from the nth to the mth module. After testing the fields on block-m, the convolution system can be established as

$$\begin{bmatrix} e^- \\ \eta h^- \end{bmatrix}_{m,j} = \sum_{k=0}^{k^c_{\max}-1} [C]_{m,k} \begin{bmatrix} e^i \\ \eta h^i \end{bmatrix}_{m,j-k} + Q^c_{m,j-k^c_{\max}} \tag{9}$$

in which

$$\begin{bmatrix} e^i \\ \eta h^i \end{bmatrix}_{m,j} = \begin{bmatrix} e^{\rm inc} \\ \eta h^{\rm inc} \end{bmatrix}_{m,j} + \sum_{m=1, m\neq n}^{M} \left\{ \sum_{k=0}^{k^{d,mn}_{\max}-1} [D]_{mn,k} \begin{bmatrix} e^- \\ \eta h^- \end{bmatrix}_{n,j-k} + Q^d_{mn,j-k^{d,mn}_{\max}} \right\} \tag{10}$$

and

$$Q^c_{m,j-k^c_{\max}} = Q^c_{m,j-k^c_{\max}} + [C]_{m,k^c_{\max}} \begin{bmatrix} e^i \\ \eta h^i \end{bmatrix}_{m,j-k^c_{\max}}$$

$$Q^d_{mn,j-k^{d,mn}_{\max}} = Q^d_{mn,j-k^{d,mn}_{\max}-1} + [D]_{mn,k^{d,mn}_{\max}} \begin{bmatrix} e^- \\ \eta h^- \end{bmatrix}_{n,j-k^{d,mn}_{\max}}.$$

Here, $[D]_{mn}$ is the discretized matrix of $[\mathcal{S}_1]_{m,n}$ and $k^{d,mn}_{\max}$ is its length. $Q^c_{m,k}$ and $Q^d_{mn,k}$ are the accumulating vectors due to the integration of time in the operators for each module and their interactions. The elements of $[D]_{mn}$ should be evaluated precisely so that the coupling interactions among different modules are transmitted accurately. It is also worthy to note that proper $[D]_{mn}$ can be obtained even when $[C]_m$ and $[C]_n$ are discretized by different time-steps. This will lead to a localized MOT system, which can provide higher flexibility.

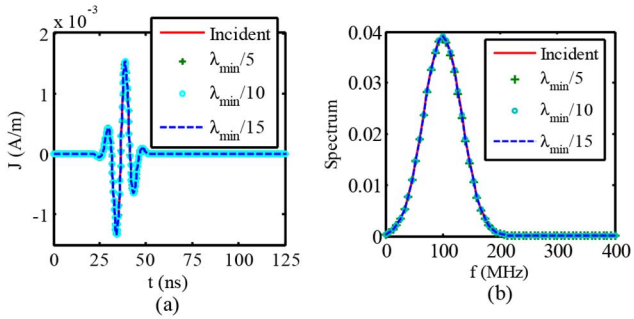

Fig. 3. Comparison of the original and reconstructed incident waves on the sphere: (a) time-domain wave form; (b) spectrums.

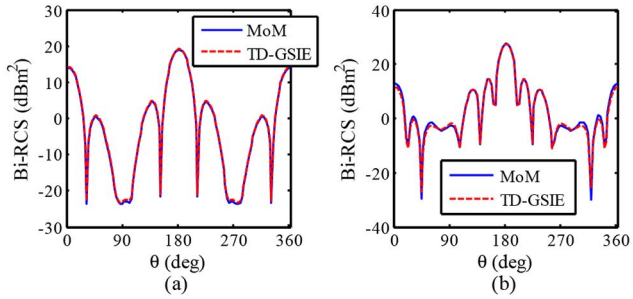

Fig. 4. Comparison of the bi-static RCSs for the 4×4 sphere array by TD-GSIE and MoM at (a) 100 MHz and (b) 150 MHz. (azimuth angle $\varphi = 0$).

IV. Numerical Results

The incident field is set to be the modulated Gaussian plane wave

$$\vec{E}^i(\vec{r},t) = \hat{p}e^{-\gamma^2}\cos(2\pi f_0\tau) \tag{11}$$

where $\gamma = (\tau - t_p)/(\sqrt{2}\sigma)$, $\tau = t - (\vec{r}\bullet\hat{k})/c$, $\sigma = 3/(2\pi f_{\rm bw})$, and $t_p = 8\sigma$. f_0 is the center frequency, $f_{\rm bw}$ is the half-bandwidth. $\hat{k}$ is the propagation direction, and $\hat{p}$ is the polarization direction. To evaluate the matrices elements, analytical scheme in [10] is adopted. The time basis function is the triangle basis.

A. Dielectric Sphere

In the first example, transient scattering from a dielectric sphere is analyzed. Radius of the sphere is 0.5 m with relative permittivity $\varepsilon_{\rm r} = 2.2$. Configurations for the incident are $f_0 = 100$ MHz, $f_{\rm bw} = 100$ MHz, $\hat{p} = -\hat{x}$, and $\hat{k} = -\hat{z}$. The sphere's mesh is composed of 2004 RWGs, with an average edge length of 0.07 m. The reference surface is a cubic around the sphere with side length 1.2 m. To get the TD-GTM of the dielectric sphere, inner MOT solver is established based on the Müller equation, with a time-step of 0.25 ns.

The discretization of the Huygens surface is a key issue for both the accuracy and efficiency of the TD-GTM. Here, we discretize the reference surface respectively with average edge length of $\lambda_{\rm min}/5$, $\lambda_{\rm min}/10$, and $\lambda_{\rm min}/15$. To show the accuracy of the reconstructed incident wave by the reference surface, we plot the tested incident electric fields on one RWG of the original sphere in Fig. 3(a) and their corresponding spectrums in Fig. 3(b).

It can be seen that the incident field can be regenerated very well using the Huygens unknowns on the reference surface even when the surface is discretized by $\lambda_{\rm min}/5$. We use this mesh configuration to extract the TD-GTM, the length of which is $k^c_{\rm max} = 100$, equivalent to $r_{\rm sl} = 2.7$. Then, we apply it to analyze a 4×4 dielectric sphere array aligned on the xy-plane. The distances between the centers of two adjacent elements in x- and y-direction are $\Delta x = 1.5$ m, $\Delta y = 1.5$ m. The accuracy of the TD-GSIE is verified through the radar cross section (RCS) comparison with method of moments (MoM) at 100 and 150 MHz in Fig. 4(a) and (b). The relative L_2 errors are both below 1.0%. However, the number of unknowns is reduced to only 17% of the original problem.

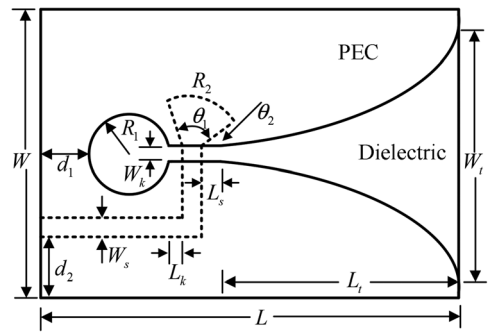

Fig. 5. Geometry parameters of the Vivaldi antenna.

B. Vivaldi Phased Antenna Array

In the last example, we analyze the transient scattering of a Vivaldi antenna array. The parameters for the incident wave are: $\hat{k} = [-\sqrt{2}/2, 0, -\sqrt{2}/2]$, $\hat{p} = [-\sqrt{2}/2, 0, \sqrt{2}/2]$, $f_0 = 2.4$ GHz, and $f_{\rm bw} = 1.2$ GHz. The geometry parameters of each antenna element are depicted in Fig. 5, which are listed as follows: $L = 12$ cm, $L_{\rm t} = 8.5$ cm, $L_{\rm s} = 0.3$ cm, $L_{\rm k} = 0.2$ cm, $W = 9$ cm, $W_{\rm t} = 7$ cm, $W_{\rm s} = 0.3$ cm, $W_{\rm k} = 0.2$ cm, $d_1 = 0.7$ cm, $d_2 = 2$ cm, $R_1 = 1$ cm, $R_2 = 1.5$ cm, $\theta_1 = 77^\circ$, $\theta_2 = 31^\circ$. The substrate's relative dielectric constant $\varepsilon_{\rm r}$ is 2.2, and its thickness is 0.4 cm. Center working frequency of the antenna is 2.4 GHz.

For this composite structure, the MOT solver is established based on the PMCHWT and EFIE, following the procedures detailed in [12]. There are 569 RWGs on the substrate and 454 RWGs on the PEC parts, of which 101 are junction functions. The average edge length of the antenna mesh is 0.9 cm. The reference surface is a cuboid measuring $13 \times 10 \times 1.4$ cm^3, with each side 0.5 cm away from the Vivaldi element. It is meshed with 354 RWGs, with an average discretization size 1.8 cm. The time-step is 0.01 ns. The length of TD-GTM is 150, equivalent to $r_{\rm sl} = 2.5$.

It takes 12.2 h and 0.43 GB memory to extract the TD-GTM matrices $[C]_k$. Then, the TD-GTM module is applied for an antenna array, whose size ranges from 2×2 to 10×10, and the distances between the centers of two adjacent elements in y- and z-direction are $\Delta y = 12$ cm, $\Delta z = 5.8$ cm, as is shown in Fig. 6.

In Table I, we list the CPU time and memory cost by the TD-GSIE and MOT solvers when filling the $[D]_k$ matrices for different array sizes. Note that since the $[D]_k$ matrices are the

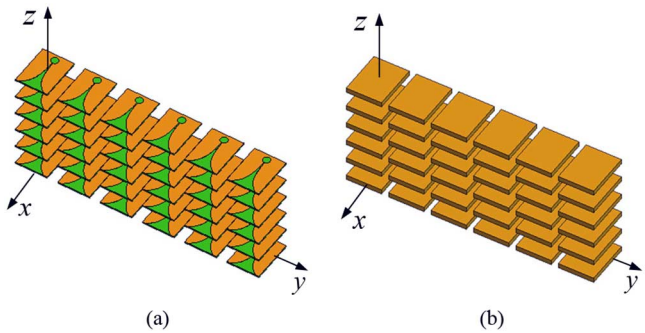

Fig. 6. Configuration for the Vivaldi antenna array (a) original structure and (b) enclosed by the Huygens surfaces.

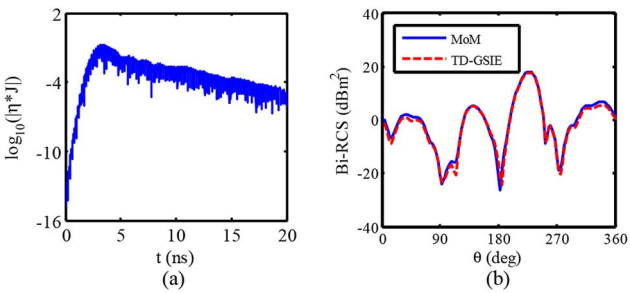

Fig. 7. Results of the 6×6 Vivaldi array: (a) currents on the reference surface of one element; (b) RCS results at 2.4 GHz (azimuth angle $\varphi = 0$).

TABLE I
COMPUTATION COST FOR THE ANTENNA ARRAY

Array size	Number of $[D]_k$ matrix	Number of unknowns TD-GSIE/MOT	$[D]_k$ filling time/memory cost for TD-GSIE	$[D]_k$ filling time/memory cost for MOT
2*2	8	2832/8184	2.2hrs/1.39GB	10.4hrs/8.9GB
4*4	48	11328/32736	13.4hrs/8.2GB	60.2hrs/42.1GB
6*6	120	25488/73656	35.1hrs/20.4GB	-
8*8	224	45312/130944	65.6hrs/37.9GB	-
10*10	360	70800/204600	108.2hrs/60.5GB	-

same if the two pairs of coupling blocks have the same relative displacement vector, we only need to calculate a minimum number of different $[D]_k$ matrices, which is specified in Table I. The TD-GSIE solver has dominant advantages in both time and memory consumption. When the array size is extended to 6×6, it is beyond the capability of our computer using the traditional MOT solver.

To show the stability and accuracy of the TD-GSIE solver, numerical results for the 6×6 array are provided. Currents of the observed RWG on the reference surface of one antenna are plotted in Fig. 7(a). RCS results at 2.4 GHz are compared to MoM in Fig. 7(b), of which the relative L_2 error is 2.1%. This error can be caused by the compression of the degree of freedom on the Huygens surfaces as well as the limited truncation length of the impulse responses. For this antenna array analysis, the method in [2] poses a great advantage for the application of the synthetic basis function (SBF) technique, which can further compress the unknowns of the reference surfaces. However, for the method in [2], series of simulations at different sampling frequencies will be needed in order to get the wideband information.

V. CONCLUSION

The TD-GTM and TD-GSIE are proposed for the transient scattering analysis of arrays. MOT solvers based on different TDIE equations like Müller, EFIE, and PMCHWT are applied to extract the TD-GTM. The TD-GSIE employing TD-GTM modules are implemented for array structures. The efficiency, accuracy, and stability of TD-GSIE are verified through numerical experiments.

REFERENCES

[1] G. Xiao, J. Mao, and B. Yuan, "A generalized surface integral equation formulation for analysis of complex electromagnetic systems," *IEEE Trans. Antennas Propag.*, vol. 57, no. 3, pp. 701–710, Mar. 2009.
[2] S. Xiang, G. B. Xiao, X. Z. Tian, and J. F. Mao, "Analysis of large-scale phased antenna array with generalized transition matrix," *IEEE Trans. Antennas Propag.*, vol. 61, no. 11, pp. 5453–5464, Nov. 2013.
[3] M. K. Li and W. C. Chew, "Wave-field interaction with complex structures using equivalence principle algorithm," *IEEE Trans. Antennas Propag.*, vol. 55, no. 1, pp. 130–138, Jan. 2007.
[4] Z. Peng, X. C. Wang, and J. F. Lee, "Integral equation based domain decomposition method for solving electromagnetic wave scattering from non-penetrable objects," *IEEE Trans. Antennas Propag.*, vol. 59, no. 9, pp. 3328–3338, Sep. 2011.
[5] A. M. van de Water, B. P. de Hon, M. C. van Beurden, A. G. Tijhuis, and P. de Maagt, "Linear embedding via Green's operators: A modeling technique for finite electromagnetic band-gap structures," *Phys. Rev. E*, vol. 72, no. 5, pp. 056704-1–11, Nov. 2005.
[6] V. Lancellotti, B. P. de Hon, and A. G. Tijhuis, "An eigencurrent approach to the analysis of electrically large 3-D structures using linear embedding via Green's operators," *IEEE Trans. Antennas Propag.*, vol. 57, no. 11, pp. 3575–3585, Nov. 2009.
[7] V. Lancellotti and A. G. Tijhuis, "Extended linear embedding via Green's operators for analyzing wave scattering from anisotropic bodies," *Int. J. Antennas Propag.*, vol. 2014, p. 11, 2014, Article ID 467931.
[8] G. Xiao, X. Tian, W. Yuan, E. Luo, and J. Fang, "Impulse responses and the late time stability properties of time-domain integral equations," *Microw., Antennas Propag.*, vol. 9, no. 7, pp. 603–610, 2015.
[9] B. Shanker, M. Lu, J. Yuan, and E. Michielssen, "Time domain integral equation analysis of scattering from composite bodies via exact evaluation of radiation fields," *IEEE Trans. Antennas Propag.*, vol. 57, no. 5, pp. 1506–1520, May 2009.
[10] X. Tian, G. Xiao, and S. Xiang, "Application of analytical expressions for retarded-time potentials in analyzing the transient scattering by dielectric objects," *IEEE Antennas Wireless Propag. Lett.*, vol. 13, pp. 1313–1316, 2014.
[11] H. A. Ülkü and A. A. Ergin, "Application of analytical retarded-time potential expressions to the solution of time domain integral equations," *IEEE Trans. Antennas Propag.*, vol. 59, no. 11, pp. 4123–4131, Nov. 2011.
[12] J. Y. Zhao, W. Y. Yin, M. D. Zhu, and W. Luo, "Time domain EFIE-PMCHW method combined with adaptive marching-on-in order procedure for studying on time- and frequency-domain responses of some composite structures," *IEEE Trans. Electromagn. Compat.*, vol. 55, no. 6, pp. 1220–1230, Dec. 2013.